Supporting Information

Electronic Structural Origin of the Catalytic Activity Trend of Transition Metals for Electrochemical Nitrogen Reduction

Byung Chul Yeo,[1,‡] Jimin Kong,[2,‡] Donghun Kim,[1] William A. Goddard III,[3] Hyun S. Park,[2,] and Sang Soo Han[1,*]*

[1]Computational Science Research Center, Korea Institute of Science and Technology (KIST), 5 Hwarangno 14-gil, Seoul 02792, Republic of Korea

[2]Fuel Cell Research Center, Korea Institute of Science and Technology (KIST), 5 Hwarangno 14-gil, Seoul 02792, Republic of Korea

[3]Materials and Process Simulation Center, California Institute of Technology, Pasadena, California 91125, United States

‡These authors contributed equally to this work.

*To whom correspondence should be addressed.

E-mail: sangsoo@kist.re.kr (SSH); hspark@kist.re.kr (HSP)

COMPUTATION SECTION

The electrochemical nitrogen reduction reaction (NRR) includes various intermediate molecules during the conversion from N_2 molecules to NH_3 molecules. In the associative NRR mechanism, there are ten intermediates, including $*N_2$, $*N_2H$, $*NNH_2$, *N, *NH, $*NH_2$, $*NH_3$, *NHNH, $*NH_2NH$, and $*NH_2NH_2$ adsorbates (Fig. S1), where * denotes a surface site. Using the density-functional theory (DFT) calculations, we examined the most stable adsorption sites for each intermediate by considering various possible geometries (Fig. S2).[S1] For $*N_2$, we considered nine adsorption sites: six horizontal alignments and three vertical ones. For $*N_2H$, *NHNH, $*NH_2NH$, and $*NH_2NH_2$, six alignments were considered. For $*NNH_2$, *N, *NH, $*NH_2$, and $*NH_3$, we considered three adsorption sites, including top, hollow, and bridge. The adsorption energies for each intermediate on Fe(110), Ru(001), Rh(111), and Pd(111) are summarized in Tables S1~S10. We obtained their thermodynamic energy profiles for the associative NRR based on the most stable geometries.

After determining the most stable configurations, we calculated the free energies of the intermediates under standard reaction conditions (pH = 0, 298 K, 1 atm) with a potential of U = 0. We estimated the chemical potential of $(H^+ + e^-)$ that is equal to that of $0.5H_2$. We considered the difference in the adsorption energies plus the free energy correction terms (zero point energy and enthalpy and entropy corrections) between the adsorbed species and the gas phase molecules.[S2] Because the correction terms of the adsorbed species were similar irrespective of metal surfaces, we used the identical values for all transition metal surfaces. The values are summarized in Table S11. Additionally, solvation effects were not included because the solvation-induced stabilization of adsorbates in the NRR is within 0.1 eV.[S3]

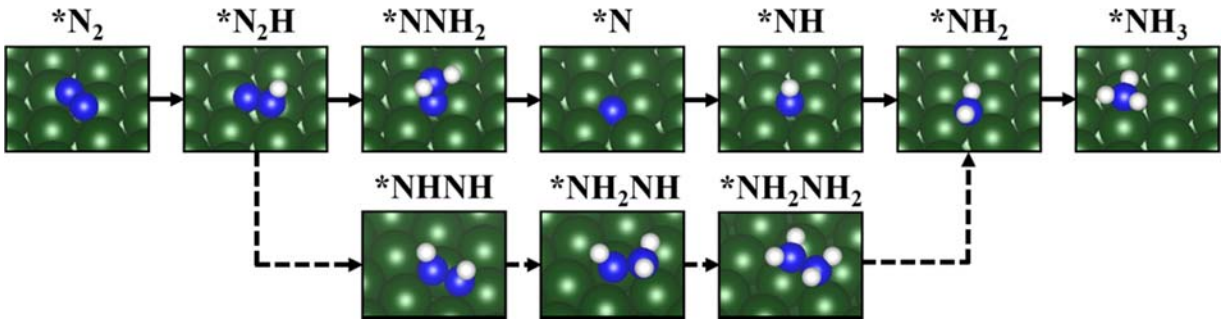

FIG. S1. Reaction intermediates in the associative NRR of N_2 to NH_3 on a transition metal surface. From the 2nd protonation, two reaction pathways are possible; i.e., $*N_2H_2$ can be either $*NNH_2$ (solid line) or *NHNH (dotted line). Blue, white, and green spheres represent N, H, and transition metal atoms, respectively.

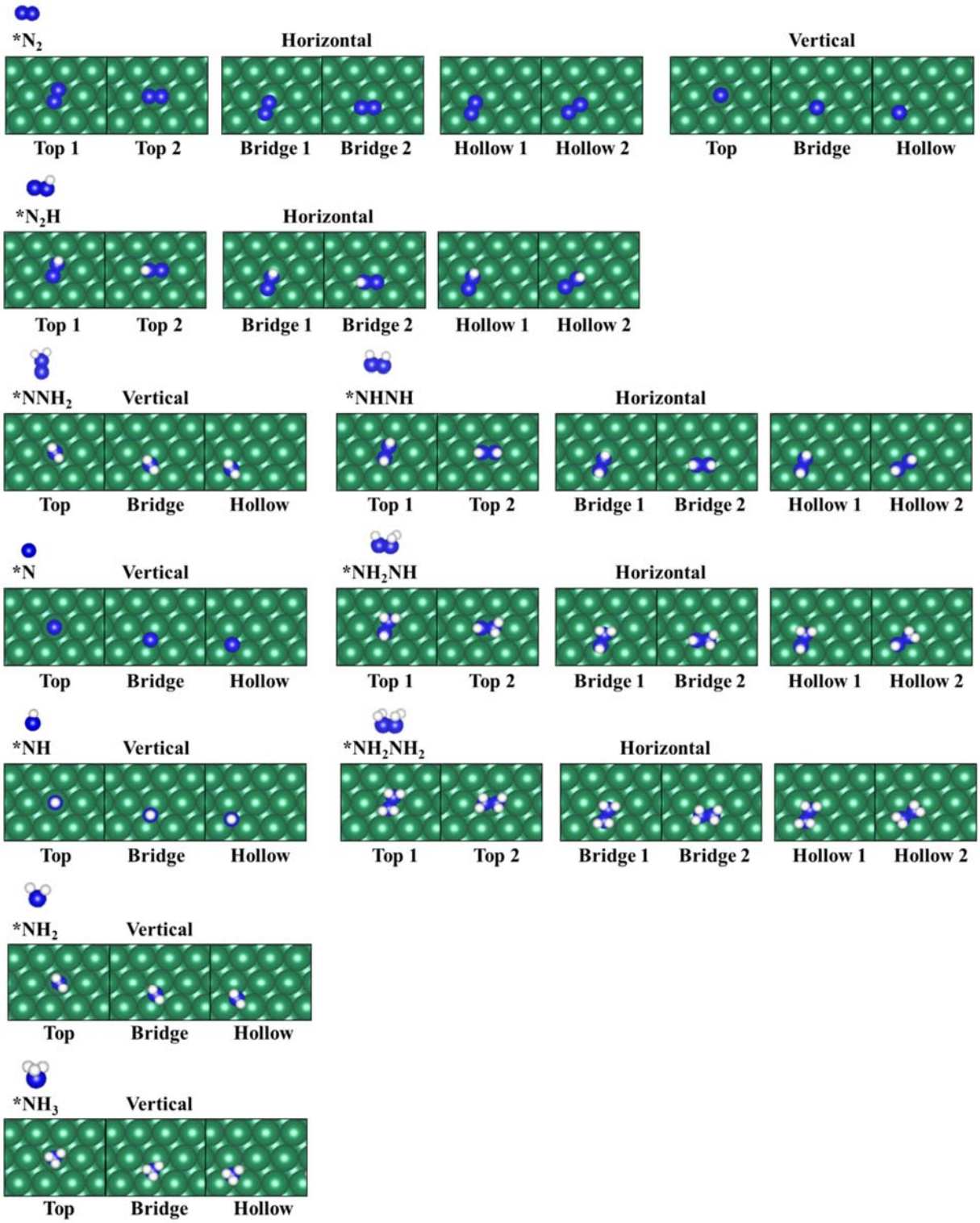

FIG. S2. Possible configurations of the intermediates (*N_2, *N_2H, *NNH_2, *N, *NH, *NH_2, *NH_3, *NHNH, *NH_2NH, and *NH_2NH_2) over transition metal surfaces.

TABLE S1. The adsorption energies ($\triangle E_{N2}$) of the $*N_2$ adsorbate on Fe(110), Ru(001), Rh(111), and Pd(111) surfaces. All values are given in eV. The adsorption energy is calculated by the following equation: $\triangle E_{N2} = E_{N2/slab} - E_{slab} - E_{N2}$.

Sites		Fe(110)	Ru(001)	Rh(111)	Pd(111)
Horizontal	Top 1	0.05	0.01	-0.15	-0.17
	Top 2	1.16	0.01	-0.15	-0.20
	Bridge 1	-0.59	-0.13	-0.26	-0.20
	Bridge 2	2.15	Unstable	-0.26	-0.20
	Hollow 1	0.67	Unstable	-0.26	-0.20
	Hollow 2	**-0.78**	Unstable	-0.15	-0.18
Vertical	Top	2.04	**-0.76**	**-0.70**	**-0.36**
	Bridge	-0.59	Unstable	Unstable	-0.13
	Hollow	4.32	Unstable	Unstable	-0.19

TABLE S2. The adsorption energies ($\triangle E_{N2H}$) of the $*N_2H$ adsorbate on Fe(110), Ru(001), Rh(111), and Pd(111) surfaces. All values are given in eV. The adsorption energy is calculated by the following equation: $\triangle E_{N2H} = E_{N2H/slab} - E_{slab} - E_{N2} - 0.5 \times E_{H2}$.

Sites		Fe(110)	Ru(001)	Rh(111)	Pd(111)
Horizontal	Top 1	Unstable	Unstable	Unstable	Unstable
	Top 2	Unstable	Unstable	Unstable	Unstable
	Bridge 1	Unstable	Unstable	Unstable	Unstable
	Bridge 2	Unstable	**0.31**	Unstable	**0.87**
	Hollow 1	**-0.32**	Unstable	Unstable	Unstable
	Hollow 2	Unstable	Unstable	**0.67**	0.97

TABLE S3. The adsorption energies ($\triangle E_{N2H2}$) of the $*N_2H_2$ adsorbate on Fe(110), Ru(001), Rh(111), and Pd(111) surfaces. All values are given in eV. The adsorption energy is calculated by the following equation: $\triangle E_{N2H2} = E_{N2H2/slab} - E_{slab} - E_{N2} - E_{H2}$.

Sites		Fe(110)	Ru(001)	Rh(111)	Pd(111)
Vertical	Top	Unstable	1.12	1.10	Unstable
	Bridge	**-0.13**	0.29	0.40	Unstable
	Hollow	Unstable	**0.20**	**0.39**	**0.80**

TABLE S4. The adsorption energies ($\triangle E_N$) of the *N adsorbate on Fe(110), Ru(001), Rh(111), and Pd(111) surfaces. All values are given in eV. The adsorption energy is calculated by the following equation: $\triangle E_N = E_{N/slab} - E_{slab} - 0.5 \times E_{N2}$.

Sites		Fe(110)	Ru(001)	Rh(111)	Pd(111)
Vertical	Top	0.11	0.71	1.64	Unstable
	Bridge	**-1.20**	Unstable	Unstable	Unstable
	Hollow	Unstable	**-1.03**	**-0.30**	**0.40**

TABLE S5. The adsorption energies ($\triangle E_{NH}$) of the *NH adsorbate on Fe(110), Ru(001), Rh(111), and Pd(111) surfaces. All values are given in eV. The adsorption energy is calculated by the following equation: $\triangle E_{NH} = E_{NH/slab} - E_{slab} - 0.5 \times E_{N2} - 0.5 \times E_{H2}$.

Sites		Fe(110)	Ru(001)	Rh(111)	Pd(111)
Vertical	**Top**	Unstable	0.74	-0.39	Unstable
	Bridge	**-1.22**	Unstable	Unstable	Unstable
	Hollow	-0.24	**-1.04**	**-0.42**	**0.26**

TABLE S6. The adsorption energies ($\triangle E_{NH2}$) of the *NH_2 adsorbate on Fe(110), Ru(001), Rh(111), and Pd(111) surfaces. All values are given in eV. The adsorption energy is calculated by the following equation: $\triangle E_{NH2} = E_{NH2/slab} - E_{slab} - 0.5 \times E_{N2} - E_{H2}$.

Sites		Fe(110)	Ru(001)	Rh(111)	Pd(111)
Vertical	**Top**	-0.07	-0.63	-0.39	0.07
	Bridge	**-0.67**	**-0.63**	**-0.39**	**0.07**
	Hollow	-0.67	-0.63	-0.39	0.07

TABLE S7. The adsorption energies ($\triangle E_{NH3}$) of the *NH_3 adsorbate on Fe(110), Ru(001), Rh(111), and Pd(111) surfaces. All values are given in eV. The adsorption energy is calculated by the following equation: $\triangle E_{NH3} = E_{NH3/slab} - E_{slab} - 0.5 \times E_{N2} - 1.5 \times E_{H2}$.

Sites		Fe(110)	Ru(001)	Rh(111)	Pd(111)
Vertical	**Top**	**0.17**	**-0.09**	**-0.07**	**0.13**
	Bridge	Unstable	Unstable	-0.07	Unstable
	Hollow	Unstable	Unstable	-0.07	Unstable

TABLE S8. The adsorption energies ($\triangle E_{NHNH}$) of the *NHNH adsorbate on Fe(110), Ru(001), Rh(111), and Pd(111) surfaces. All values are given in eV. The adsorption energy is calculated by the following equation: $\triangle E_{NHNH} = E_{NHNH/slab} - E_{slab} - E_{N2} - E_{H2}$.

Sites		Fe(110)	Ru(001)	Rh(111)	Pd(111)
Horizontal	**Top 1**	Unstable	Unstable	Unstable	1.54
	Top 2	0.02	Unstable	1.14	1.54
	Bridge 1	0.54	Unstable	0.61	Unstable
	Bridge 2	Unstable	Unstable	0.81	**1.24**
	Hollow 1	**-0.27**	**0.06**	0.81	1.29
	Hollow 2	Unstable	0.19	**0.60**	1.25

TABLE S9. The adsorption energies ($\triangle E_{NH2NH}$) of the *NH_2NH adsorbate on Fe(110), Ru(001), Rh(111), and Pd(111) surfaces. All values are given in eV. The adsorption energy is calculated by the following equation: $\triangle E_{NH2NH} = E_{NH2NH/slab} - E_{slab} - E_{N2} - 1.5 \times E_{H2}$.

Sites		Fe(110)	Ru(001)	Rh(111)	Pd(111)
Horizontal	**Top 1**	Unstable	Unstable	Unstable	Unstable
	Top 2	Unstable	Unstable	0.56	1.17
	Bridge 1	Unstable	Unstable	0.56	0.99
	Bridge 2	1.36	Unstable	Unstable	Unstable
	Hollow 1	1.23	Unstable	Unstable	1.05
	Hollow 2	**0.31**	**-0.05**	**0.27**	**0.97**

TABLE S10. The adsorption energies ($\triangle E_{NH2NH2}$) of the *NH_2NH_2 adsorbate on Fe(110), Ru(001), Rh(111), and Pd(111) surfaces. All values are given in eV. The adsorption energy is calculated by the following equation: $\triangle E_{NH2NH2} = E_{NH2NH2/slab} - E_{Substrate} - E_{N2} - 2 \times E_{H2}$.

Sites		Fe(110)	Ru(001)	Rh(111)	Pd(111)
Horizontal	**Top 1**	Unstable	Unstable	Unstable	0.36
	Top 2	Unstable	Unstable	**0.63**	**0.85**
	Bridge 1	Unstable	Unstable	Unstable	0.36
	Bridge 2	**0.85**	**0.38**	Unstable	0.30
	Hollow 1	1.63	Unstable	Unstable	0.21
	Hollow 2	2.29	Unstable	Unstable	Unstable

TABLE S11. The zero-point energy correction (ZPE), enthalpy correction (H), entropy correction (-TS), and free energy correction (G_{corr}) for free gaseous molecules and reaction intermediates in the associative NRR process. All values are given in eV. The free energy correction is obtained by the following equation: G_{corr} = ZPE + H - TS.

Species	ZPE	H	-TS	G_{corr}
N_2 (g)	0.15	0.09	-0.58	-0.34
H_2 (g)	0.27	0.09	-0.42	-0.06
NH_3 (g)	0.93	0.10	-0.55	0.48
***H**	0.16	0.01	-0.01	0.16
***N_2**	0.20	0.09	-0.18	0.11
***N_2H**	0.48	0.07	-0.13	0.42
***N_2H_2**	0.80	0.08	-0.16	0.72
***N**	0.09	0.02	-0.03	0.08
***NH**	0.38	0.03	-0.04	0.37
***NH_2**	0.69	0.05	-0.08	0.66
***NH_3**	1.02	0.08	-0.20	0.90
***HNNH**	0.80	0.07	-0.12	0.75
***H_2NNH**	1.16	0.07	-0.12	1.11
***H_2NNH_2**	1.47	0.10	-0.18	1.39

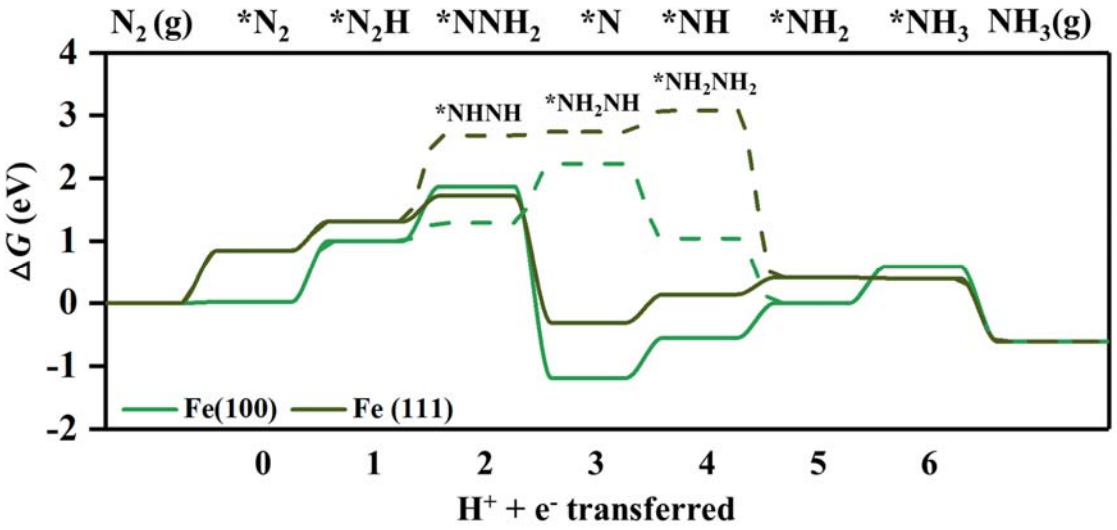

FIG. S3. Free energy diagram at U=0 V (vs. RHE) for the reaction intermediate in the associative NRR process of N_2 to NH_3 on the Fe(100) (green) and Fe(111) (black). The free energy pathway consists of 7 consecutive steps for proton-coupled electron transfers from $*N_2$ to $*NH_3$. Here, from the 2nd protonation, two reaction pathways are possible; i.e., $*N_2H_2$ can be either $*NNH_2$ (solid line) or *NHNH (dotted line).

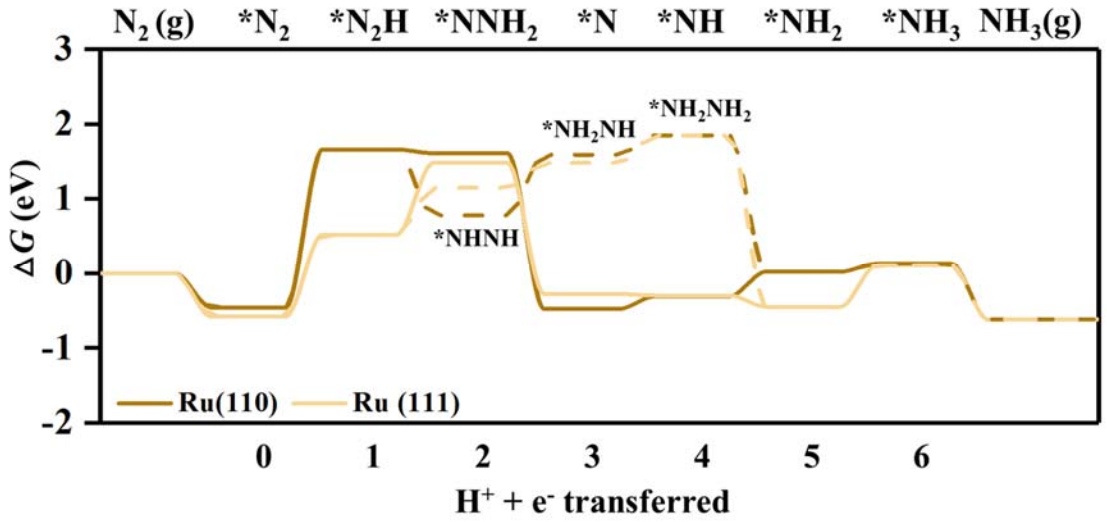

FIG. S4. Free energy diagram at U=0 V (vs. RHE) for the reaction intermediate in the associative NRR process of N_2 to NH_3 on the Ru(110) (brown) and Ru(111) (yellow). The free energy pathway consists of 7 consecutive steps for proton-coupled electron transfers from $*N_2$ to $*NH_3$. Here, from the 2nd protonation, two reaction pathways are possible; i.e., $*N_2H_2$ can be either $*NNH_2$ (solid line) or *NHNH (dotted line).

EXPERIMENT SECTION

We measured practical ammonia formation rates via an electrochemical synthesis experiment for the estimation of catalytic activities on Fe, Ru, Pd, and Rh catalysts. The TM catalysts were purchased as metallic catalysts. Fe (cubic, 99.5%, Sigma-Aldrich), Rh (cubic, 99.9%, Sigma-Aldrich), Ru (hexagonal, 99.9%, Alfa Aesar) and Pd (cubic, Sigma-Aldrich) powders were purchased and used after reductive thermal treatments as described below. All of the nanoparticles presented a circular shape (Fig. S5) as observed under the electron microscope, and they dominantly possessed the most stable surface structures.[S4] The electrochemical ammonia synthesis was carried out in a single-cell environment. The anion exchange membrane (FAA-75, Fumatec.) was used in an electrolytic cell. Rh, Ru, Pd, and Fe were investigated as the cathode catalyst, and IrO_2 was fixed as an anode catalyst. The catalyst ink consisted of catalyst powder, isopropyl alcohol, deionized water (18 MΩ) and polytetrafluoroethylene binder (60 wt% dispersion in H_2O, Sigma-Aldrich). The ink slurry was sprayed onto carbon paper (TGP-H-120, Toray) in the case of a cathode catalyst, and IrO_2 ink was used to spray on Ti paper (250 μm thickness). All of the catalyst-coated substrates (CCSs) with 2.5 x 2.5 cm^2 were thermally treated in an Ar atmosphere at 350 °C for 5 minutes at a rate of 1 °C/min. The MEA (membrane electrode assembly) was assembled with an anion exchange membrane electrolyte embedded between the cathode and the anode CCS after the heat treatment. Humidified N_2 gas was fed to the cathode at a flow rate of 200 sccm, and 0.5 M KOH solution was supplied to the anode at a flow rate of 1 mL min^{-1}. The experimental was performed at 338 K. NH_3 was electrochemically synthesized using chronoamperometry as an electrochemical measurement with a potentiostat (SI 1287, Solartron). The produced NH_3 was trapped in 100 mL of a 10 mM H_2SO_4 solution; after that, the concentration of NH_4^+ in the trap solution was determined by colorimetric measurement with the Nessler's method using UV-vis spectroscopy (Agilent, Cary 100, Fig. S6). In the Nessler's method, a calibration curve was obtained with 10 mM H_2SO_4 used as a stripping solution mixed with known amounts of NH_4OH and a commercial Nessler's reagent (K_2HgI_4, Sigma-Aldrich). The amount of NH_3 produced was investigated at various different voltages employing different cathode catalysts. Chronoamperometry (CA) was used to synthesize NH_3 at each different cell voltage for 1 hr. In the colorimetric analysis, the background signal was corrected by subtracting the absorbance for a pure 10 mM H_2SO_4 solution at 700 nm. The absorbance peak at approximately 375 nm was used to qualitatively measure NH_3. However, it appears that the applied voltage displaying the maximum NH_3 production rate under the given reaction conditions of this study was 1.3 V_{cell} for the studied electrode. Then, the NRR rates of NH_3 production rates at the catalyst surface were normalized based on Brunauer-Emmett-Teller (BET, Micrometrics ASAP 2000) surface measurements. Before use in BET measurements, the metallic catalysts were dried at 70°C for 2 hr, then ramped to 200 °C and held at this temperature overnight.

The rate of ammonia formation was calculated from the equation given by:

$$r_{NH3} = \frac{[NH4^+] \times V}{t \times A} \text{ (mol/s·cm}^2{}_{BET}\text{)} \quad \textbf{(S1)}$$

where $[NH_4^+]$ is the measured concentration of produced NH_3 in the aqueous trap solution, t is the collection time for the NRR, V is the total volume of the trap solution and A is the BET surface area of the catalyst powder.

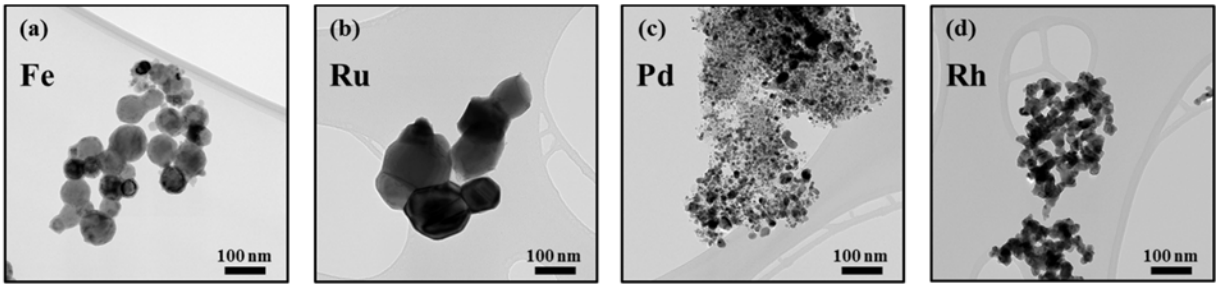

FIG. S5. TEM analysis of (a) Fe, (b) Ru, (c) Pd, and (d) Rh nanoparticles used in the electrochemical ammonia synthesis. The bar in each figure corresponds to a scale of 100 nm.

The physical and chemical properties of the catalyst surface are crucial factors that determine the catalytic activity of electrodes. As discussed above, different catalysts of metallic surface were purchased and heat-treated under a reductive atmosphere, i.e., Ar at 350 °C. Further, the metallic surfaces of Pd, Ru, and Rh are thermodynamically stable, as shown in Pourbaix diagrams in Fig. S11. For Fe, the catalyst surface is also considered the metal catalyst; thin surface native oxide, possibly formed at ambient atmosphere, is removed to reveal the metal surfaces in performing electrochemical reductive reactions.[S7-S12] In this study, a dominant hydrogen evolution reaction (HER) in addition to the NRR is observed, which reduce the dinitrogen or proton to NH_3 and H_2 at negative potentials, and the metallic Fe catalyst surfaces are reported for the HER [S7-S12]. In addition, we performed the NRR experiment using fully oxidized Fe (Fe_2O_3) nanoparticles to investigate the effect of the oxide on the NH_3 formation as the reviewer mentioned. In the experiment, the ammonia synthesis rate of Fe_2O_3 was 4.6 x 10^{-14} mol s^{-1} cm^{-2} $_{BET}$ at 1.6 V cell, which is much less than that of Fe metal surfaces (2.35 x 10^{-13} mol s^{-1} cm^{-2} $_{BET}$). In the comparison, we considered the similar particle sizes of Fe_2O_3 and Fe; i.e., the particle size distributions of Fe_2O_3 and Fe are 45~90 nm and 40~70 nm, respectively. Because the ammonia synthesis rate over Fe_2O_3 is significantly lower than that over Fe, the catalytic activity reported in Table 1 can be regarded as a result for Fe rather than for Fe_2O_3.

Fe nanoparticles which reveal in the air are very vulnerable to oxidation before BET measurements. For studying oxidation of Fe by air, we investigated the oxide thickness of water-

pretreated Fe surface and air-pretreated Fe surface using QUASES Analyze. In case of air-pretreated Fe surface for 1 min (dose ~5 x 10^{10}L), the thickness of oxide was 3.2 nm; the figure is significantly larger than the water-pretreated Fe surface. Then, the oxide layer consists of hydroxides or oxyhydroxides regardless of the reaction conditions.[S13] Since the thickness of the oxide layer (3.2 nm) occurred by the atmospheric exposure is much less than the particle size of Fe (45-90 nm), the oxidation of Fe nanoparticles doesn't significantly affect to the BET measurement. Assuming that Fe was completely oxidized to Fe_2O_3, we measured the surface area of commercial Fe_2O_3 (Aldrich) which is similar to the particle size of the catalyst used in the experiment. By the BET analysis, the surface area of Fe_2O_3 is 34 m^2/g, whereas the surface area of Fe (oxidized surface) is 10 m^2/g. Therefore, it is possible to underestimate ammonia synthesis rate of Fe nanoparticles in our experiment because the activity of catalyst is normalized by larger value than the actual surface area.

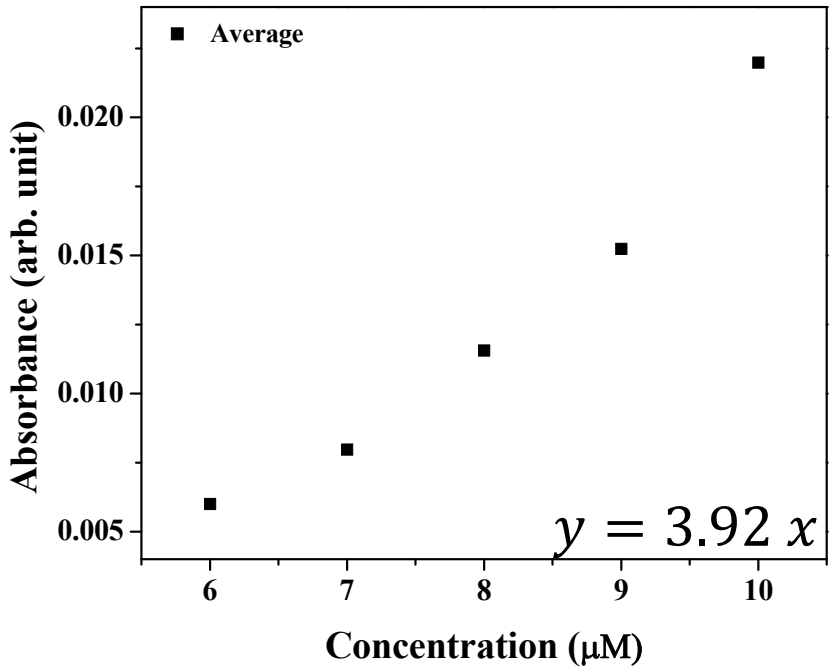

FIG. S6. Calibration curve for Nessler's method.

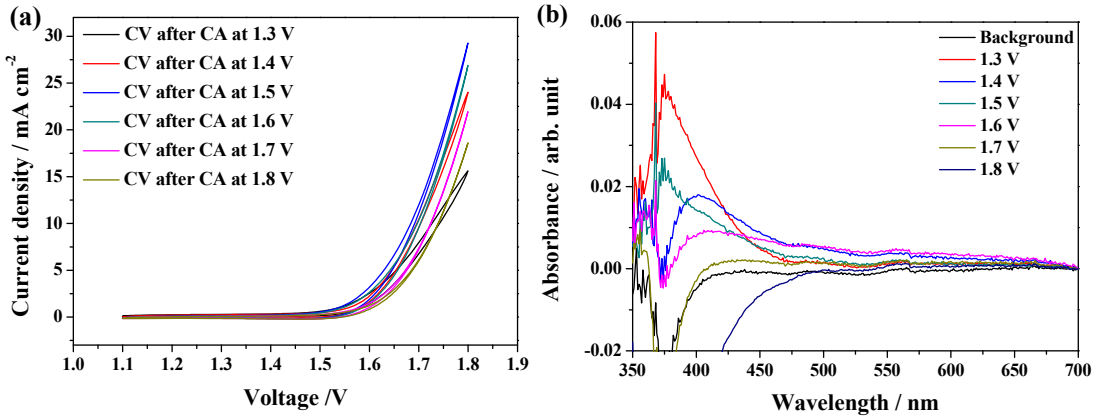

FIG. S7. (a) Cyclic voltammogram from a single cell device with Fe-coated carbon paper and IrO_2-coated titanium paper into the cathode and anode, respectively. (b) UV-vis spectrum obtained via Nessler's method with 10 mM H_2SO_4 used as a trapping solution to determinate NH_3 produced during CA at different cell voltages. The solution used as background in the UV-vis spectrum is pure 10 mM H_2SO_4.

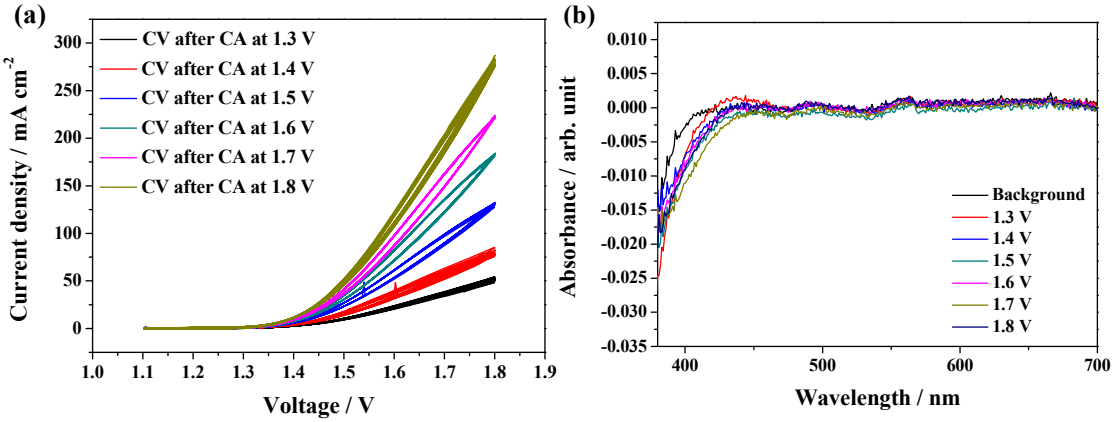

FIG. S8. (a) Cyclic voltammogram from a single cell device with Rh-coated carbon paper and IrO_2-coated titanium paper into the cathode and anode, respectively. (b) UV-vis spectrum obtained via Nessler's method with 10 mM H_2SO_4 used as a trapping solution to determinate NH_3 produced during CA at different cell voltages. The solution used as background in the UV-vis spectrum is pure 10 mM H_2SO_4.

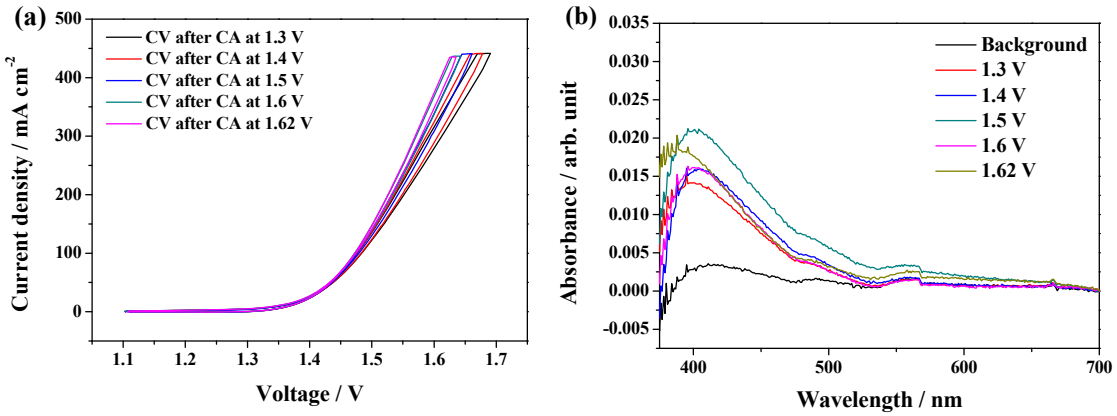

FIG. S9. (a) Cyclic voltammogram from a single cell device with Ru-coated carbon paper and IrO_2-coated titanium paper into the cathode and anode, respectively. (b) UV-vis spectrum obtained via Nessler's method with 10 mM H_2SO_4 used as a trapping solution to determinate NH_3 produced during CA at different cell voltages. The solution used as background in the UV-vis spectrum is pure 10 mM H_2SO_4.

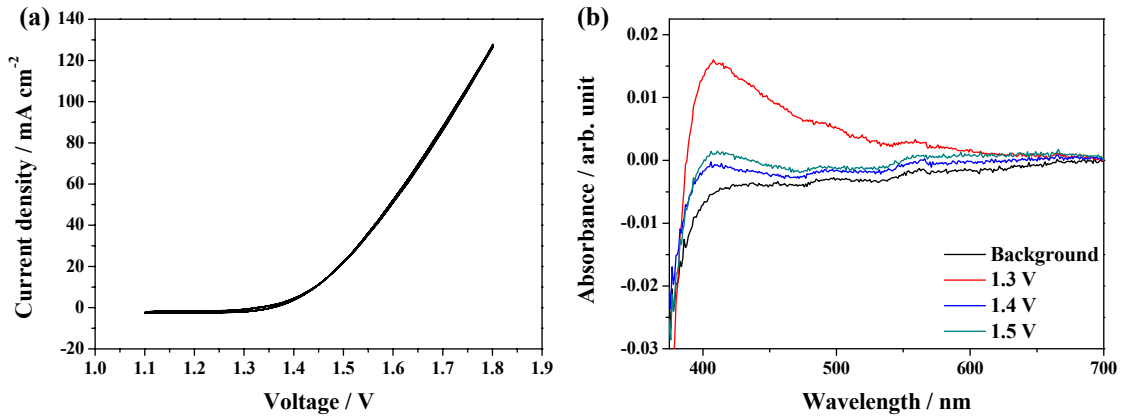

FIG. S10. (a) Cyclic voltammogram from a single cell device with Pd-coated carbon paper and IrO_2-coated titanium paper into the cathode and anode, respectively. (b) UV-vis spectrum obtained via Nessler's method with 10 mM H_2SO_4 used as a trapping solution to determinate NH_3 produced during CA at different cell voltages. The solution used as background in the UV-vis spectrum is pure 10 mM H_2SO_4.

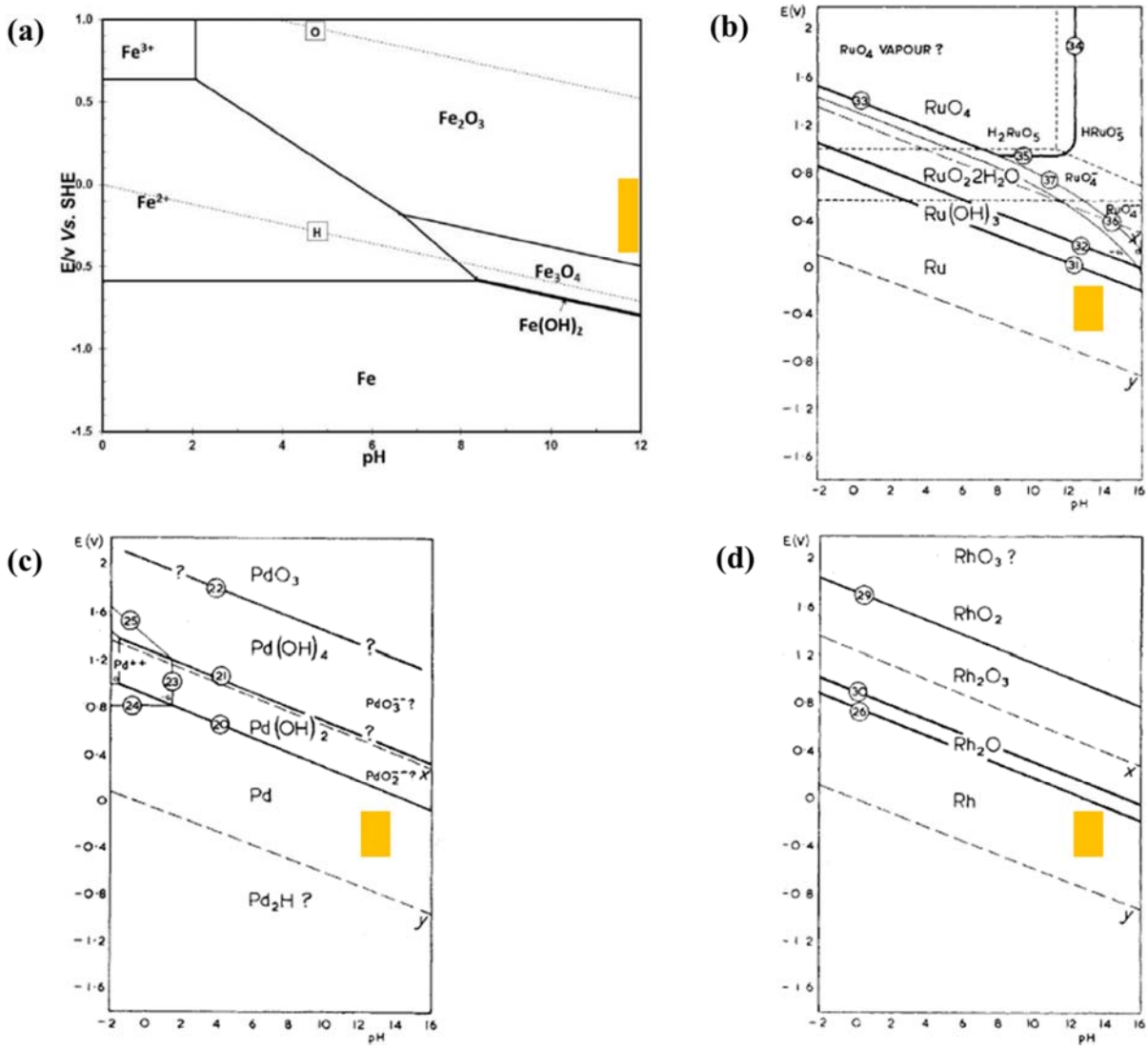

Fig. S11. Pourbaix diagrams of (a) Fe, (b) Ru, (c) Pd, and (d) Rh. The yellow mark displays the region where electrochemical measurements were performed in this study. The diagram of Fe is reproduced with permission from reference S6. Copyright 2015 NACE International. And, the diagrams of Ru, Pd, and Rh are reproduced with permission from reference S5. Copyright 1959 Johnson Matthey.

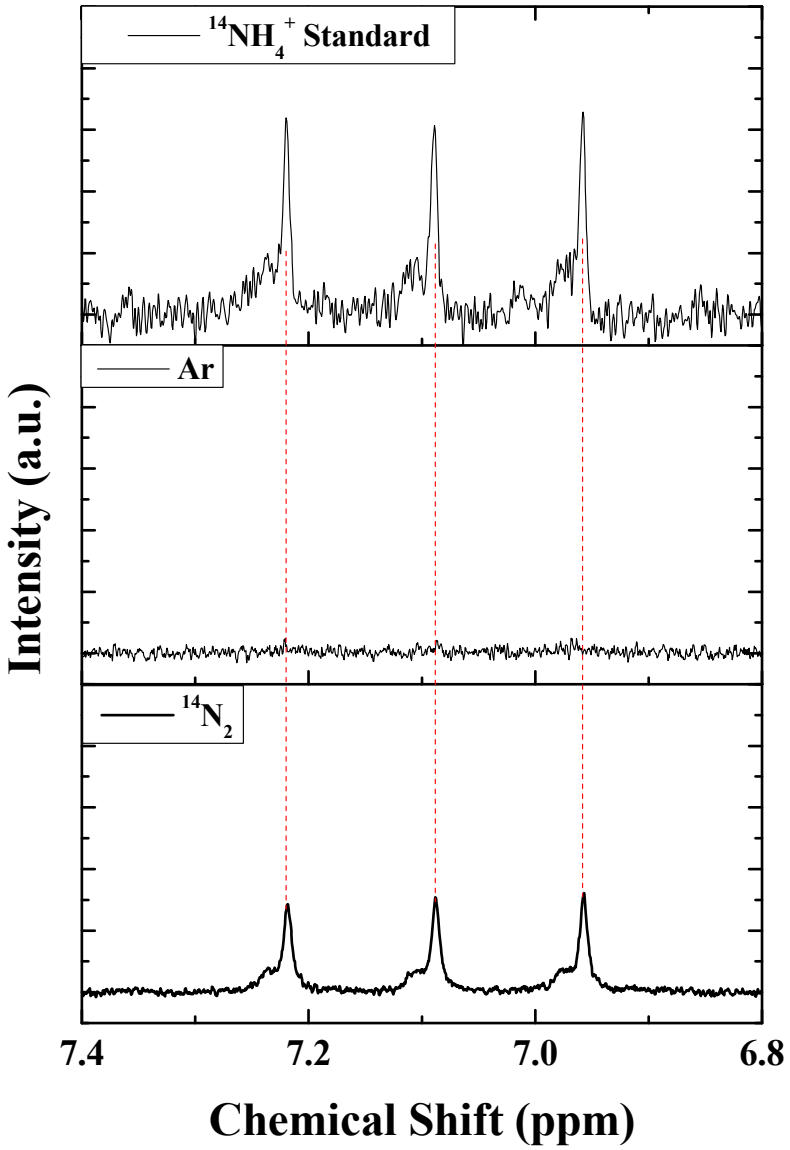

Fig. S12. The 1H NMR Spectra of NH_4^+ produced form electrochemical reduction using $^{14}N_2$ (bottom) and Ar (middle) as the feeding gas including that of NH_3 standard solution using NH_4OH (top). For the NMR measurement, the N_2-electrolysis was performed at Pd/C electrode at -0.3 V_{RHE} in N_2-saturated 0.1 M KOH electrolyte for 1 h.

REFERENCES

(S1) Yeo, S. C.; Han, S. S.; Lee, H. M. Adsorption, Dissociation, Penetration, and Diffusion of N_2 on and in BCC Fe: First-Principles Calculations. *Phys. Chem. Chem. Phys.* **2013**, *15*, 5186-5192.
(S2) Skúlason, E.; Bligaard, T.; Gudmundsdóttir, S.; Studt, F.; Rossmeisl, J.; Abild-Pedersen, F.; Vegge, T.; Jónsson, H.; Nørskov, J. K. A Theoretical Evaluation of Possible Transition Metal Electro-Catalysts for N_2 Reduction. *Phys. Chem. Chem. Phys.* **2012**, *14*, 1235-1245.
(S3) Montoya, J. H.; Tsai, C.; Vojvodic, A.; Nørskov, J. K. The Challenge of Electrochemical Ammonia Synthesis: A New Perspective on the Role of Nitrogen Scaling Relations. *ChemSusChem.* **2015**, *8*, 2180-2186.
(S4) Liu, X.; Wen, X.; Hoffmann, R. Surface Activation of Transition Metal Nanoparticles for Heterogeneous Catalysis: What We Can Learn from Molecular Dynamics. *ACS Catal.* **2018**, *8*, 3365-3375.
(S5) Pourbaix, M. J. N.; Van Muylder, J.; de Zoubov, N. Electrochemical Properties of the Platinum Metals. *Platinum Metals Rev.* **1959**, *3*, 47-53.
(S6) Ning, J.; Zheng, Y.; Brown, B.; Young, D.; Nesic, S. Construction and Verification of Pourbaix Diagrams for Hydrogen Sulfide Corrosion of Mild Steel. *Corrosion* **2015**, *71*, 946-960.
(S7) Pentland, N.; Bockris, J. O'M.; Sheldon, E. Hydrogen Evolution Reaction on Copper, Gold, Molybdenum, Palladium, Rhodium, and Iron. *J. Electrochem. Soc.* **1957**, *104*, 182-194.
(S8) Devanathan, M. A. V.; Stachurski, Z. The Mechanism of Hydrogen Evolution on Iron in Acid Solutions by Determination of Permeation Rates. *J. Electrochem. Soc.* **1964**, *111*, 619-623.
(S9) Lasia, A.; Rami, A. Kinetics of Hydrogen Evolution on Nickel Electrodes. *J. Electroanal. Chem.* **1990**, *294*, 123-141.
(S10) Kibria, M. F.; Mridha, M. S.; Khan, A. H. Electrochemical Studies of a Nickel Electrode for the Hydrogen Evolution Reaction. *Int. J. Hydrogen Energy* **1995**, *20*, 435-440.
(S11) Müller, C. I.; Rauscher, T.; Schmidt, A.; Schubert, T.; Weißgärber, T.; Kieback, B.; Röntzsch, L. Electrochemical Investigations on Amorphous Fe-base Alloys for Alkaline Water Electrolysis. *Int. J. Hydrogen Energy* **2014**, *39*, 8926-8937.
(S12) Franceschini, E. A.; Lacconi, G. I.; Corti, H. R. Kinetics of the Hydrogen Evolution on Nickel in Alkaline Solution: New Insight from Rotating Disk Electrode and Impedance Spectroscopy Analysis. *Electrochm. Acata* **2015**, *159*, 210-218.
(S13) Grosvenor, A. P.; Kobe, B. A.; McIntyre, N. S. Studies of the Oxidation of Iron by Air After Being Exposed to Water Vapor Using Angle-Resolved X-Ray Photoelectron Spectroscopy and QUASES. *Surf. Interface Anal.* **2004**, *36*, 1637-1641.